Short Communication

Construction of TiO$_2$/Si Heterostructure by Nanoepitaxial Growth of Anatase-type TiO$_2$

Liguo Gao[1,], Yanqiang Li[1], Qun Li[1], Hanlin Chen[1], Tingli Ma[2,*]*

[1] State Key Laboratory of Fine Chemicals, School of petroleum and chemical engineering, Dalian University of Technology, Panjin, 124221, China.
[2] Graduate School of Life Science and Systems Engineering, Kyushu Institute of Technology, 2–4 Hibikino, Wakamatsu, Kitakyushu, Fukuoka 808–0196, Japan.
[*] E-mail: liguo.gao@dlut.edu.cn, tinglima@dlut.edu.cn

Nearly defect-free interfaces can be formed using two lattice-matched semiconductors and nanoepitaxial growth methods that can be controlled at the atomic level. In this work, the nanoepitaxy of anatase-type TiO$_2$ on crystalline silicon substrates for fabricating TiO$_2$/Si heterogeneous interface is demonstrated by combining self-assembly and hydrothermal methods. Solid-phase nanoepitaxy is formed in this heterogeneous interface according to the crystal type and crystal lattice matching between anatase-type TiO$_2$ and crystalline silicon. X-ray diffraction (XRD) and crystal symmetry indicate that the nanoepitaxy growth of anatase-type TiO$_2$ on the Si (001) plane is (001) plane. Anatase-type TiO$_2$ atoms are directly connected with Si atoms. Inconsiderable SiO$_2$ exists between anatase-type TiO$_2$ and crystalline silicon substrate. These interfaces could promote the transfer rate of carriers and decrease the recombination rate of hole–electron pairs. This evidence is confirmed by comparison with rutile-type TiO$_2$, which could not be grown on Si substrate due to the mismatching crystal lattice parameter. The rutile-type TiO$_2$ can be removed easily in ultrasonic condition.

1. INTRODUCTION

Almost a defect-free heterogeneous interface is formed by crystal-face-induced nanoepitaxial growth, in which two different materials are connected directly through chemical bonding according to lattice matching.[1–4] Such a heterogeneous interface is widely used in various fields, such as in fabricating surface plasmon resonance devices,[5–7] improving magnetic properties,[8–10] and photoelectrochemical (PEC) water splitting[11,12], given its characteristics of excellent charge transfer

capacity and ferroelectric properties at the interface. Construction methods of heterogeneous interface connection can be divided into three types: bridging linker, layer-by-layer assembly, and synthesis of nanocrystals in solution or in gas phase. Miljevic et al.[13] combined Au and TiO_2 nanocrystals through bridging linker method by using bifunctional groups to improve photocatalytic efficiency. Yamada et al.[14] deposited nanocrystal CeO_2 onto the surface of Pt nanoparticles by layer-by-layer assembly method and prepared a heterogeneous interface with CeO_2-Pt connection, which increased its catalytic activity. Ibánezetal et al.[15] combined PbTe of epitaxial growth and PbS that was fabricated by the epitaxial growth of PbTe on PbS nanocrystals in solution, thereby forming a PbTe–PbS core/shell nanocomposite with high electric conductivity and low thermal conductivity.

Heterogeneous interface is crucial to the design of PEC devices. Semiconductor silicon is used as the substrate, and a metal-oxide-semiconductor heterogeneous interface is constructed, which will serve as transistor[16] and interface for PEC water splitting.[17–20] Common metallic oxides include $Mg_2Al_2O_4$[21], MgO[22], and TiO_2[18,23]. However, the existence of SiO_2 on silicon surface forms a large potential barrier against passing through of electrons and restricts the electron–hole transfer at the interface. Therefore, direct nanoepitaxial growth on silicon surface can effectively reduce the electron–hole combination on the interface and increase the transfer rate of carriers, thereby improving the photoelectric property. Li et al.[12] reported that the lattice constant of cubic perovskite $SrTiO_3$ matches well with the Si(001) surface unit cell and developed nearly defect-free interfaces successfully on the silicon surface through the epitaxial growth of molecular beam. Sahasrabudhe et al. connected one layer of amorphous TiO_2 on the silicon surface of H:Si under vacuum and low-temperature conditions through a series of vapor depositions.[24]

Research has proven that anatase-type TiO_2 crystal possesses higher electron–hole transfer capacities than amorphous TiO_2 does.[25,26] In this study, anatase-type TiO_2 growth is induced on the (001) surface of n-type monocrystalline Si by layer-by-layer assembly method and nanoepitaxial growth. Anatase-type TiO_2 can be directly grown on the silicon surface due to the two lattice-matched semiconductors. Comparison with the synthesis experiments of rutile nanorod on silicon surface confirm that only anatase-type TiO_2 with matched crystal type and lattice can grow on silicon surface. The PEC test indicates that the prepared TiO_2/Si sample has basically the same onset potential and saturation photocurrent density as monocrystalline Si.

2. EXPERIMENTAL SECTION

2.1 Materials

The Si wafers [n type, (100)] were obtained from Youyan Guigu Beijing, China. Ni wire (99%) were purchased from Tmall used as received. Titanium tetrachloride, tetrabutyl titanate, Hydrochloric acid (HCl), Hydrogen fluoride (HF), Glacial acetic, hydrogen peroxide (H_2O_2), ethanol, chloroform, and acetone were purchased from commercial sources at the highest available purity and used without further purification. The compact TiO_2 agent used for spin-coating was purchased from Sigma Aldrich.

2.2 Preparation of Silicon Substrates

Silicon wafer was cut into 1.5*1.5 cm^2 slices and washed in an ultrasonic bath (240 W) with acetone, chloroform, ethanol, deionized (DI) water about 5 min, respectively. Then, Si wafers was soaked in a 1:1:5 (by volume) solution of ammonia solution (25%), hydrogen peroxide (H$_2$O$_2$, 30%) and DI water for 60 min at 80℃. They are washed in an ultrasonic bath with DI water for 5 min. To remove SiO$_2$, Si wafers were put in a 3:1 (by volume) solution of H$_2$O, and hydrogen fluoride (40%) for 5 min. They were put into ethanol absolute rapidly after removing SiO$_2$.

2.3 Nanoexpitaxial of Anatase-type TiO$_2$

For nanoepitaxial growth anatase-type TiO$_2$ process, the Si wafers were firstly dipped in titanium tetrachloride for 1 min. Then, they were washed in ultrasonic bath with DI water for 1 min. A clean process with ethanol solution was carried out before dipping the Si wafers into titanium tetrachloride again. This progress was prepared by repeating eight times from dipping in titanium tetrachloride to washing with ethanol solution to grow a connecting layer on Silicon substrate. Glacial acetic, tetrabutyl titanate and DI water with a volume ratio of 30:0.5:0.4 was added in Teflon-lined autoclave and heated at 140℃ for 8 h. After the hydrothermal process, the samples were collected and washed with DI water. Finally, the samples were annealed at 250℃ for 2 h with 5℃/min heating rate in N$_2$ atmosphere. Then, they cooled at room temperature.

2.4 Nanoexpitaxial of Rutile-type TiO$_2$

For nanoepitaxial growth rutile-type TiO$_2$ process, the Si wafers were firstly dipped in titanium tetrachloride for 1 min. Then, they were washed in ultrasonic bath with DI water for 1 min. A clean process with ethanol solution was carried out before dipping the Si wafers into titanium tetrachloride again. This progress was prepared by repeating eight times from dipping in titanium tetrachloride to washing with ethanol solution. Hydrochloric acid (15 mL, 6M) was well dissolved into 15 mL DI water under magnetic stirring to get solution A. Then, 0.5 mL tetrabutyl titanate was taken using the pipetting to dissoved into the above solution to get solution B. The Silicon substate and solution B were added in Teflon-lined autoclave and heated at 150℃ as reported by others[30]. After the hydrothermal process, the samples were collected and washed with DI water. Finally, samples were annealed at 250℃ for 2 h with 5℃/min heating rate in N$_2$ atmosphere. Then, they cooled at room temperature.

2.5 Preparation of anatase-type TiO$_2$ (Spin-coating)/Si

Before spin-coating TiO$_2$, the Si wafers were prepared as 4.2 description. Then, they were dipped in titanium tetrachloride for 1 min and washed in ultrasonic bath with DI water for 1 min. A clean process with ethanol solution was carried out before dipping the Si wafers into titanium

tetrachloride again. This progress was prepared by repeating eight times from dipping in titanium tetrachloride to washing with ethanol solution to grow a connecting layer on Silicon substrate. A compact TiO_2 agent was spin-coated onto the Si substrates, which were sequentially annealed at 450 °C for 30 min.

2.6 Catalyst Ni deposited

Ni film was deposited onto TiO_2/Si substrates by a thermal deposition process. During the deposition process, the system was maintained under a pressure of 10^{-4} Pa and at a rate of 0.03 Å/S. Ohmic contacts to the back sides of TiO_2/Si samples were formed by evaporating Ag onto the unpolished surface with 20 nm thicknesses.

2.7 Characterization

The surface morphology was determined by SEM on a Nova NanoSEM 450 (FEI). The lattice structure was observed under a HRTEM at an accelerating voltage of 200 kV (HRTEM, Tecnai G2 F20). The chemical compositions of the samples were analyzed by EDS, which is equipped on HRTEM. The crystal structure of the samples were studied by XRD (XRD-7000S) using Cu KR radiation from 20° to 80° at a scanning speed of 5°/min. All electrochemical experiments were performed on CHI630D electrochemical work station in air at room temperature. All electrolyte solutions prepared with DI water. A saturated calomel electrode was used as the reference electrode. Pt wire was used as the counter electrode for all electrochemical measurements performed in 1.0 M KOH (aq) electrolyte. The linear sweep voltammetry curves were measured at 100 mV/S without iR compensation. During the measurement, the electrolyte was vigorously stirred with a magnetic stir bar driven by a model-train motor. A Xenon arc lamp was used as the light source. Illumination was provided by an AM 1.5G solar simulator, and the intensity was adjusted to 100 mW/cm^2 by the standard silicion cell. All the electrodes in this study were typically 0.2 cm^2 in area. All measured potentials were converted to the NHE reference scale using $E_{(NHE)} = E_{(SCE)} + 0.2415V$.

3. RESULTS AND DISCUSSION

The unit cell structures of monocrystalline Si and anatase-type TiO_2 are shown in Fig. 1. Monocrystalline Si belongs to face-centered cubic structure. On the crystal face (100) of monocrystalline Si, square is formed by four Si atoms. In each square, two Si atoms are on the face center of two adjacent units, and the other two Si atoms are at the vertex angle. The length of Si−Si bonds is 0.3840 nm. The anatase-type TiO_2 belongs to tetragonal structure. The square is formed by four Ti atoms on its (001) crystal face. The length of Ti−Ti bonds is 0.3784 nm, which is only 0.0056 nm shorter than the length of Si−Si bonds on (100), thereby showing a small lattice mismatching degree of only 1.46%. The anatase-type TiO_2 and monocrystalline Si present a high matching degree of crystal type and lattice. The theoretical calculation implies that the in-situ growth of anatase-type

TiO_2 on monocrystalline Si surface is possible. Studies have shown that only crystals with matched lattice and crystal form can be crystal-face-induced nanoepitaxial grown. Hojo et al. demonstrated well-aligned heterogeneous interfaces by selectively nucleating anatase-type TiO_2 in a one-on-one fashion and grown epitaxially on a nanocrystalline monolayer of CeO_2.[4] The anatase-type TiO_2 grew uniformly along the [001] direction on the (001) surfaces of CeO_2 nanocubes. Strontium titanate, $SrTiO_3$, can be grown epitaxially on Si (001) with minimal interfacial reactions.[27] The lattice constant of a cubic perovskite $SrTiO_3$ (3.905 Å) matches well with the Si (001) surface unit cell (3.84 Å), which results in a small (–1.7%) lattice mismatch with $SrTiO_3$/Si and low interface state density. It creates a nearly perfect electrical interface.[28] Ji et al. revealed a thin epitaxial layer of $SrTiO_3$ grew directly on Si(001) by molecular beam epitaxy to form an metal–insulator–semiconductor photocathode, where the photogenerated electrons can be transported easily through $SrTiO_3$ layer and result in a high photon-to-current efficiency.[12]
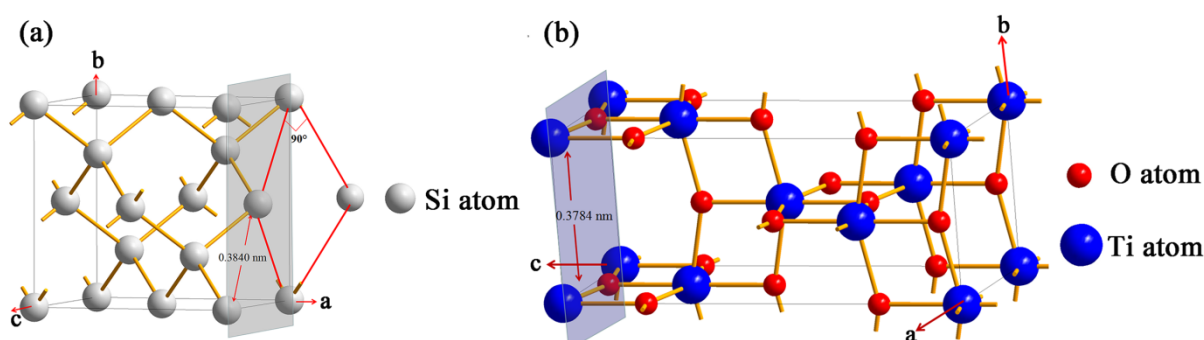
Figure 1. Schematic crystal structure (a) Si unit cell; (b) Anatase-type TiO_2 unit cell

The scanning electron microscopy (SEM) image in Fig. 2a shows that anatase-type TiO_2 nanoparticles distribute on monocrystalline Si surface in a single layer. A high-resolution image of the nanoepitaxial growth is obtained through high-resolution transmission electron microscopy, which is shown as insert image of Fig. 2a. Symmetry analysis demonstrates that anatase-type TiO_2 and Si are dual symmetry. These two surfaces are (101) face. Further analysis on the lattice parameters of anatase-type TiO_2 presents that the distance between one vertex of dual-symmetric rhombus and the diagonal is 0.2468 nm, which proves that the horizontal contact surface between anatase-type TiO_2 and monocrystalline Si is the (001) surface because the top face of our monocrystalline Si is (001) face. The type of crystal structure is analyzed through XRD in Fig. 2b. A characteristic diffraction peak of monocrystalline Si substrate is obtained at $2\theta=54°$. The peak at $2\theta=25°$ is the characteristic peak of anatase-type TiO_2 (101), which indicates the successful synthesis of anatase-type TiO_2 crystals on the monocrystalline Si surface. The small peak intensity is caused by the quantity of TiO_2 nanoparticles on the substrate surface.
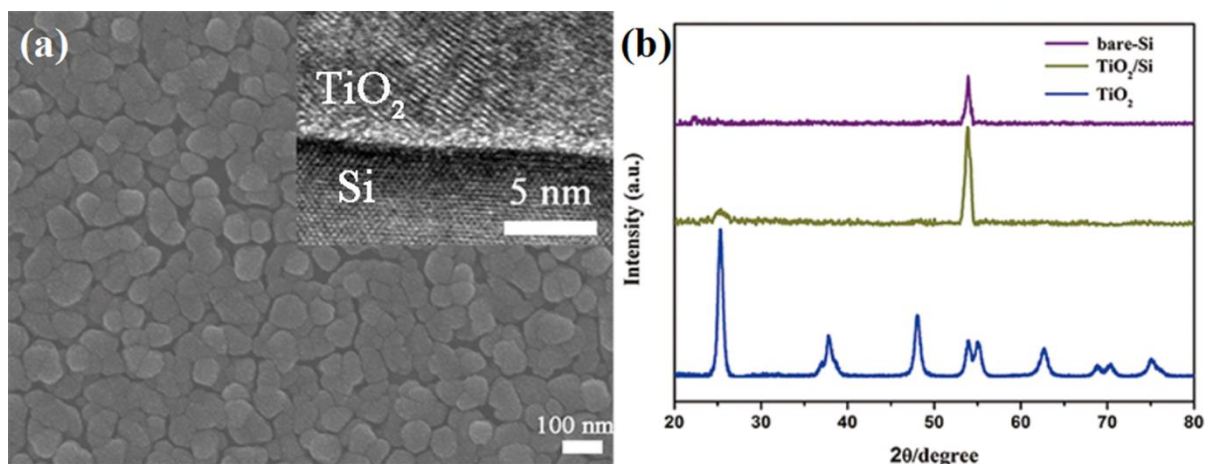
Figure 2. (a) SEM image of Anatase-type TiO_2 nanoepitaxy on Si substrate, the insert is HRTEM profile image of TiO_2/Si heterogeneous interface; (b) XRD pattern of Si, Si/TiO_2 and TiO_2

The induction of rutile-type TiO_2 by monocrystalline Si is compared in this study to further verify that anatase-type TiO_2 and monocrystalline Si have matched crystal type and lattice and only crystals with matched lattice and crystal form can be crystal-face-induced nanoepitaxial grown. The growth period of rutile-type TiO_2 is shown in Fig. 3. Rutile-type TiO_2 is rod crystal, and rod-shaped TiO_2 grows gradually on the side as the hydrothemal synthesis continues, thereby forming flower-like TiO_2. The XRD analysis shown in Fig. 3d proves that the prepared rod-shaped TiO_2 is rutile-type TiO_2 and that its characteristic peak is at $\theta=27.4°$[28]. The lattice constants of the unit cell of rutile are $a=b=0.4594$ nm and $c=0.2959$ nm, which disagree with those of monocrystalline Si. Therefore, rutile cannot have nanoepitaxial growth on monocrystalline Si. The nanorod rutile-type TiO_2 in Fig. 3a is also easy to be peeled off from the monocrystalline Si surface by ultrasonic processing.
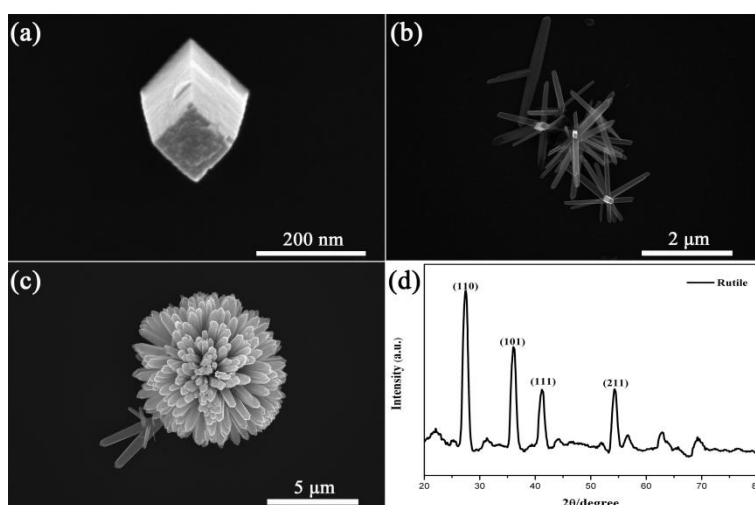
Figure 3. Rutile-type TiO_2 nanorod with different hydrothermal time (a) 1h, (b) 3h, (c) 8h; (d) XRD pattern of Rutile-TiO_2
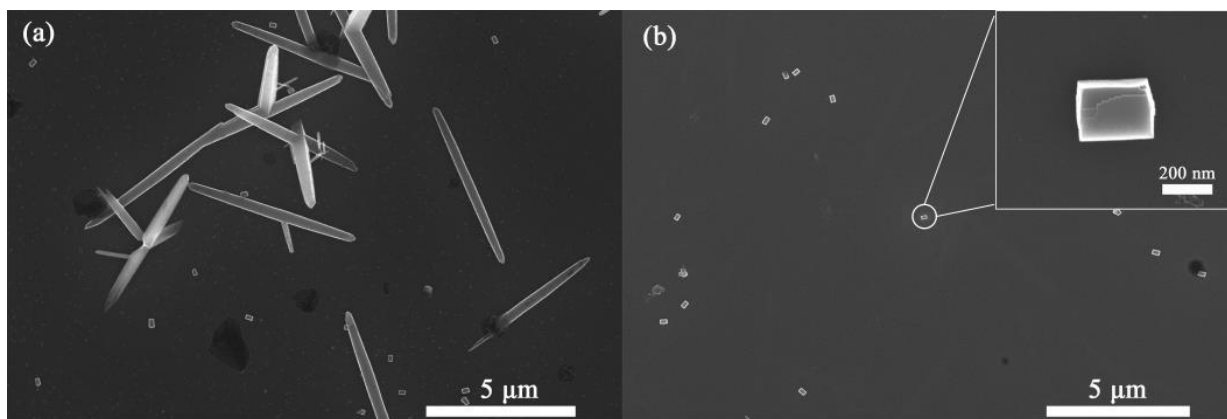
Figure 4. SEM image of rutile-TiO_2 nanorod on Si substrate, (a) without ultrasonic treatment; (b) with ultrasonic treatment; the insert is a magnified SEM image of anatase-type TiO_2.

Anatase-type TiO_2 still could be seen on the silicon surface after nanorod rutile-type TiO_2 is peeled off by ultrasonic processing shown in Fig. 4. This anatase-type TiO_2 grows at the silicon substrate surface by crystal induction and cannot be removed by ultrasonic processing. The amplification illustration in Fig. 4b depicts that this square TiO_2 is different from nanorod rutile-type TiO_2 and has not been reported yet. Hence, although rutile-type TiO_2 is the precondition for TiO_2 synthesis, anatase-type TiO_2 still could grow on silicon surface due to the induction of monocrystalline Si surface. However, the anatase-type TiO_2 is square and has a small quantity.
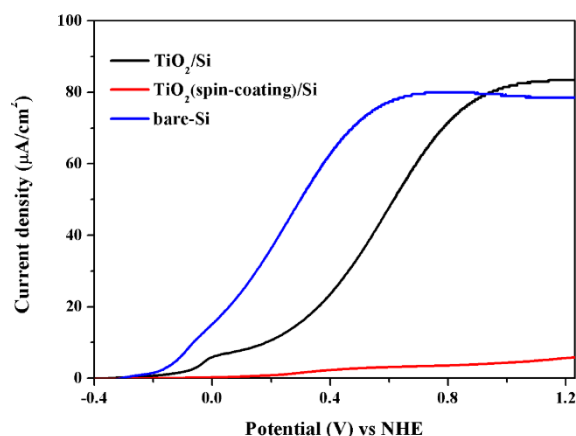
Figure 5. Liner sweep voltammograms from TiO_2/Si, TiO_2(spin-coating)/Si and bare-Si sample

The anatase-type TiO_2/Si heterostructure has high hole transfer capacity. Ni, a non-noble metal with chemical stability, has been used as a catalyst deposited through the chemical vapor deposition (CVD) for 1 nm. The PEC properties of anatase-type TiO_2/Si heterostructure exposed to different substrates (bare-Si, anatase-type TiO_2/Si, and anatase-type TiO_2 (Spin-coating)/Si) are compared (Fig. 5). The spin-coating thickness is the same as the TiO_2 thickness of nanoepitaxial growth. The results demonstrate that the TiO_2/Si heterostructure has 0.4 V lower threshold voltage and 20 times higher photocurrent density under 1.23 V voltage (standard electrode potential for H_2O oxidation) than TiO_2 (Spin-coating)/Si substrate. Compared with Si substrate, the TiO_2/Si heterostructure has basically the

same onset potential and photocurrent density. The applied voltage at the maximum photocurrent is relatively high, which is related to the TiO_2 film thickness. In other words, the PEC properties of Si change slightly after the nanoepitaxial growth of TiO_2. Therefore, the TiO_2/Si heterostructure can use TiO_2 to protect Si and avoid corrosion of monocrystalline Si in solution without influencing Si properties. This heterostructure has great application potentials in the photoanode of PEC water splitting.

4. CONCLUSIONS

Nanoepitaxial growth of TiO_2 of anatase-type TiO_2 on the (001) surface of monocrystalline Si is achieved by combining layered self-assembly and hydrothermal synthesis, which is attributed to their lattice and crystal type matching. The conditions for growth of nanorod rutile-type TiO_2 prove that lattice and crystal type matching are the preconditions for nanoepitaxial growth of crystal heterogeneous interface; otherwise, nanoepitaxial growth is impossible, and the heterogeneous interface is easy to be peeled off from the surface. Nanoepitaxial growth TiO_2 on monocrystalline Si surface has high transfer capacity of carriers and basically the same PEC properties with monocrystalline Si. Its saturation photocurrent density is 20 times higher than that of TiO_2 (Spin-coating)/Si substrate.

References

1. J.W. Reiner, A.M. Kolpak, Y. Segal, K.F. Garrity, S. Ismail-Beigi, C.H. Ahn, and F.J. Walker, *Adv. Mater.*, 22 (2010) 2919.
2. D. K. Fork, D.B. Fenner, G.A.N. Connell, J.M. Phillips, and T.H. Geballe, *Appl. Phys. Lett.*, 57 (1990) 1137.
3. J.M. Bao, *Nature. Nanotech.*, 10 (2015) 19.
4. D. Hojo, T. Togashi, T. Ohsawa, M. Saito, Z.C. Wang, Y. Sakuda, S. Asahina, Y. Ikuhara, T. Hitosugi, and T. Adschiri, *Cryst. Growth Des.*, 14 (2014) 4714.
5. H.L. Chen, H.C. Cheng, T.S. Ko, S.Y. Chuang, and T.C. Chu, *Jpn. J. Appl. Phys.*, 45 (2006) 6984.
6. G.A. Sotiriou, A.M. Hirt, P.Y. Lozach, A. Teleki, F. Krumeich, and S.E. Pratsinis, *Chem. Mater.*, 23 (2011) 1985.
7. A. Tanaka, A. Ogino, M. Iwaki, K. Hashimoto, A. Ohnuma, F. Amano, B. Ohtani, and H. Kominami, *Langmuir*, 28 (2012) 13105.
8. H. Yu, M. Chen, P.M. Rice, S.X. Wang, R.L. White, and S. Sun, *Nano lett.*, 5 (2005) 379.
9. X.L. Sun, N.F. Huls, A. Sigdel, and S.H. Sun, *Nano lett.*, 12 (2012) 246.
10. T.D. Schladt, T. Graf, O. Köhler, H. Bauer, M. Dietzsch, J. Mertins, R. Branscheid, U. Kolb, and W. Tremel, *Chem. Mater.*, 24 (2012) 525.
11. Y.C. Pu, G. Wang, K.D. Chang, Y. Ling, Y.K. Lin, B.C. Fitzmorris, C.M. Liu, X.H. Lu, Y. Tong, J.Z. Zhang, Y.J. Hsu, and Y. Li, *Nano lett.*, 13 (2013) 3817.

12. L. Ji, M.D. McDaniel, S.J. Wang, A.B. Posadas, X.H. Li, H.Y. Huang, J.C. Lee, A.A. Demkov, A.J. Bard, J.G. Ekerdt, and E.T. Yu, *Nature Nanotech.*, 10 (2015) 84.
13. M. Miljevic, B. Geiseler, T. Bergfeldt, P. Bockstaller, and L. Fruk, *Adv. Funct. Mater.*, 24 (2014) 907.
14. Y. Yamada, C.K. Tsung, W. Huang, Z. Huo, S.E. Habas, T. Soejima, C.E. Aliaga, G.A. Somorjai and P. Yang, *Nat. Chem.*, 3 (2011) 372.
15. M. Ibáñez, R. Zamani, S. Gorsse, J. Fan, S. Ortega, D. Cadavid, J.R. Morante, J. Arbiol, and A. Cabot, *ACS nano*, 7 (2013) 2573.
16. K. Eisenbeiser, J.M. Finder, Z. Yu, J. Ramdani, J.A. Curless, J.A. Hallmark, R. Droopad, W.J. Ooms, L. Salem, S. Bradshaw, and C.D. Overgaard, *Appl. Phys. Lett.*, 76 (2000) 1324.
17. K. Sun, S. Shen, J.S. Cheung, X. Pang, N. Park, J. Zhou, Y. Hu, Z. Sun, S.Y. Noh, C.T. Riley, P.K.L. Yu, S. Jin, and D. Wang, Phy. *Chem. Chem. Phys.*, 16 (2014) 4612.
18. Y.W. Chen, J.D. Prange, S. Dühnen, Y. Park, M. Gunji, C.E.D. Chidsey, and P.C. McIntyre, *Nat. Mater.*, 10 (2011), 539.
19. K. Sun, X. Pang, S. Shen, X. Qian, J.S. Cheung, and D. Wang, *Nano lett.*, 13 (2013) 2064.
20. J. Feng, M. Gong, M.J. Kenney, J.Z. Wu, B. Zhang, Y. Li, and H. Dai, *Nano. Res.*, 8 (2015) 1577.
21. M. Ihara, Y. Arimoto, M. Jifuku, T. Kimura, S. Kodama, H. Yamawaki, and T. Yamaoka, *J. Electrochem. Soc.*, 129 (1982) 2569.
22. D.K. Fork, F.A. Ponce, J.C. Tramontana, and T.H. Geballe, *Appl. Phys. Lett.*, 58 (1991) 2294.
23. M.T. McDowell, M.F. Lichterman, A.I. Carim, R. Liu, S. Hu, B.S. Brunschwig, and N.S. Lewis, *Appl. Mater. Inter.*, 7 (2015) 15189.
24. G. Sahasrabudhe, S.M. Rupich, J. Jhaveri, A.H. Berg, K.A. Nagamatsu, G. Man, Y.J. Chabal, A. Kahn, S. Wagner, J.C. Sturm and J. Schwartz., *J. Am. Chem. Soc*., 137 (2015) 14842.
25. A.G. Scheuermann, J.P. Lawrence, A.C. Meng, K. Tang, O.L. Hendricks, C.E.D. Chidsey and P.C. Mclntyre, *Appl. Mater. Inter.*, 8 (2016) 14596.
26. B. Ohtani, Y. Ogawa, and S.J. Nishimoto, *J. Phys. Chem. B*, 101 (1997) 3746.
27. M.P. Warusawithana, C. Cen, J.C. Woicik, Y. Li, L.F. Kourkoutis, J.A. Klug, P. Ryan, L.P. Wang, M. Bedzyk, D.A. Muller, L.Q. Chen, J. Levy, and D.G. Schlom, Science, 324 (2009) 367.
28. R.A. McKee, F.J. Walker, and M.F. Chisholm, Science, 293 (2001) 468.
29. Y. Xing, and X. Ding, *J. Appl. Polym. Sci.*, 103 (2007) 3113.
30. J. Cai, J. Ye, S. Chen, X. Zhao, D. Zhang, S. Chen, Y. Ma, S. Jin, and L. Qi, *Energ. Environ. Sci.*, 5 (2012) 7575.